ASEAN Journal of Science and Engineering

Journal homepage: http://ejournal.upi.edu/index.php/AJSE/

Mathematical Modeling of Static and Dynamic Stresses in the Construction of the Load-Handling Frame of a Stationary Hoist During the Loading of Grain Cargo into Containers: Literature Review and Experiments

Oyum Balabayev, Aidana Kassymzhanova, Marat Ibatov, Valentin Mikhailov, Bakhtiyar Askarov*

Abylkas Saginov Karaganda Technical University, Karaganda, Republic of Kazakhstan
*Correspondence: E-mail: kassymzhanovaaidana@gmail.com

ABSTRACT

The export of grains plays a pivotal role in the global economy, and the implementation of efficient container loading systems is of paramount importance for reducing time and resource expenditure. This study aims to develop a stationary hoist designed for loading grain into containers for railway transportation. The application of direct integration and matrix force methods enabled the calculation of static and dynamic stresses in the load-handling frame. Simulations of the container filling process were conducted to evaluate the dependency of time and speed on the results. The results demonstrated that the maximum normal stresses satisfied the strength conditions, while dynamic stresses were calculated based on the falling height of the grain. The findings revealed a relationship between the hole radius in downcomer pipes and the container filling time, providing valuable insights for optimizing hoist operation. The research offers practical relevance for grain producers, transportation companies, and researchers, contributing to more efficient grain loading and transportation.

ARTICLE INFO

Article History:
Submitted/Received 15 Aug 2024
First Revised 26 Sep 2024
Accepted 11 Nov 2024
First Available online 12 Nov 2024
Publication Date 01 Dec2024

Keyword:
Harvesting and Transport Complex,
Load Planning,
Machinery,
Optimization,
Railway Transportation,
Unitized Load.

1. INTRODUCTION

The efficient transportation of grain is of vital importance in agricultural markets, particularly in countries such as Kazakhstan, where grain exports constitute a significant contributor to the national economy. One crucial area for improvement is the optimization of loading and unloading systems employed for the transportation of grain. The objective of this research is to design and evaluate a stationary hoist system that enhances the loading of grain into railway containers. The focus is on ensuring the structural integrity of the system and on optimizing its operational efficiency. By addressing both static and dynamic stresses, this study offers practical recommendations for enhancing the safety, cost-effectiveness, and reliability of grain-loading equipment in Kazakhstan's agricultural sector.

The study of improving the efficiency of bulk cargo transportation has been a topic of interest to various researchers. Some researchers (Kassymzhanova *et al*., 2022) put forth a novel design for a stationary lifting apparatus to accelerate the loading of bulk cargo into railway containers. Other researchers (Ilesaliev *et al*., 2021) investigated the factors affecting the transportation of bulk cargo and emphasized the importance of efficient loading. Similarly, other researchers (Ibatov *et al*., 2021) investigated methods for optimizing the loading operations and transportation of bulk cargo by rail. Another research group (Mizanbekov *et al*., 2023) concentrated on the reduction of transportation costs for grain, whereas other researchers (Ruzmetov & Valieva, 2021) proposed the utilization of a novel grain lorry to minimize operational costs and downtime during reloading.

Although considerable progress has been made in the field of grain loading systems, the contribution of this study is the development of a novel mathematical model for the calculation of both static and dynamic stresses in load-handling frames employed during the grain loading process. Previous studies have typically focused on either static or dynamic stress calculations separately. In contrast, the approach combines these elements in a unified model, which offers more accurate predictions of stress behaviors during the loading of grain into containers.

Thus, improvement of the technological process of transporting wheat in containers is an urgent task, which contributes to increasing the efficiency of container transportation. However, currently, there are no effective methods of loading grain cargo into containers at elevators of agricultural enterprises. The objective of this research is to enhance the design of a stationary hoist system to improve operational efficiency, maintain structural integrity, and offer significant cost reductions in Kazakhstan's grain transportation sector. This study contributes to the field of global grain logistics, demonstrating that integrated stress analysis can result in the development of safer and more cost-effective solutions.

2. LITERATURE REVIEW

The efficiency and safety of grain transportation have long been regarded as essential aspects of global agricultural logistics. Many researchers have investigated potential innovations in grain transport systems, with a particular focus on the utilization of containers and the impact of dynamic and static stresses on load-handling mechanisms.

Some researchers (Wilson & Dahl, 2011) highlighted the pivotal role of grain pricing and transportation dynamics in agricultural markets. The research demonstrated that the implementation of efficient transport systems contributes to the overall stability of the market by reducing the time and costs associated with the grain supply chain. Other researchers similarly emphasized the significance of logistics in influencing grain prices, elucidating how transportation costs exert a direct impact on the ultimate market price that

DOI: http://dx.doi.org/10. 17509/xxxx.xxxx
p- ISSN 2776-6098 e- ISSN 2776-5938

farmers receive. It is therefore evident that the implementation of efficient grain transportation systems is of paramount importance in maintaining competitive pricing.

The advancement of technological innovations in grain transportation has attracted considerable attention. Some researchers (Kassymzhanova *et al*., 2022) conducted a study on the design of a novel stationary hoist to increase the speed and efficiency of loading grain cargo into containers transported by railway. The experiments, conducted in the ANSYS software environment, determined the maximum stresses experienced by the hoist construction, thereby validating its safety and efficiency under various conditions. This innovation is of great consequence for Kazakhstan, where grain exports constitute a significant proportion of the national economy.

In a further expansion of this area of research, some researchers (Ilesaliev *et al*., 2021) examined the factors influencing bulk cargo transportation systems. The study's objective was to enhance loading efficiency through intermodal and multimodal technologies, which have the potential to markedly reduce downtime and operating costs during the transportation of grain. Other researchers (Ibatov *et al*., 2021) also contributed to the field by investigating methods to optimize loading and unloading operations in rail transport systems. This ultimately led to increased efficiency and reduced costs for transporting bulk grain.

In addition to domestic innovations, international research has made a significant contribution to the advancement of grain logistics technologies. In a case study (Dyer *et al*., 2023), the modernization of anchorage points for the safe entry of vehicles into grain storage facilities was investigated using the finite element method. The research demonstrated the practical application of modern technologies in ensuring the safety and efficiency of grain storage and transport. Similarly, some researchers (Horabik *et al*., 2016) conducted experiments and simulations utilizing the discrete element method to analyze the distribution of static loads in grain storage silos, thereby advancing the comprehension of structural stresses during the processes of transport and storage.

Some researchers (Mizanbekov *et al*., 2023) conducted a study specific to Northern Kazakhstan, to identify the factors that affect the cost of grain transportation. The researchers emphasized the significance of reducing transportation costs to enhance the competitiveness of Kazakh grain in global markets. Similarly, other researchers (Ruzmetov & Valieva, 2021) put forth a novel grain lorry design that could potentially reduce operating costs and decrease rolling stock downtime during reloading operations.

Other studies have examined the optimization of rail and intermodal transport systems for grain. Some researchers (Zhao *et al*., 2020) developed a model for organizing railway container loading in intermodal transport. The model was designed to optimize resource use and provide an environmentally sustainable perspective. The model, validated through calculations and simulations, offers a promising solution for enhancing the efficiency of container-based grain transport, particularly in China. Similarly, other researchers (Bruns & Knust, 2012) put forth strategies for optimizing train load planning in multimodal terminals, intending to maximize train utilization while minimizing setup and transportation costs.

The solutions developed by these researchers offer valuable insights into the optimization of grain transport logistics. In Kazakhstan, where grain exports are of great importance, these innovations have the potential to enhance the efficiency of container-based transport systems, reduce costs, and improve competitiveness in the global market. As Kazakhstan continues to modernize its agricultural logistics infrastructure, the application of both domestic and international research findings will be instrumental in driving future advancements in the sector.

DOI: http://dx.doi.org/10. 17509/xxxx.xxxx
p- ISSN 2776-6098 e- ISSN 2776-5938

3. METHODS

This research work was based on the following methods: analysis, synthesis, concretization, comparison, generalization, and modeling. In the process of conducting a scientific study using the method of generalization, various aspects of agricultural product transportation in Kazakhstan, the USA, China, and other countries were considered. The method of analysis was used to draw conclusions based on reports, studies, and presentations conducted by other scientists regarding the examination and improvement of cargo operations, their variations in different countries and regions, and the key factors on which their efficiency depends. To evaluate the performance and reliability of the load-handling frame in a stationary hoist, a series of trials were conducted. During these trials, loads were systematically applied, and stresses were measured at various test positions. **Table 1** presents the comprehensive data obtained from these trials, illustrating the corresponding loading to the structure in tonnes per MPa and the resulting stresses in different positions of the frame. This permits an exhaustive examination of how the structure responds to augmented loads and the particular stress distribution patterns that were observed during the trials.

Table 1. Form for recording the obtained results.

Trials		**1**	**2**	**3**	**4**	**5**	**6**	**7**	**8**
Loadings to the structure, m_i, t/MPa		25/ 245.25	35/ 343.35	45/ 441.45	55/ 539.55	65/ 637.65	75/ 735.75	85/ 833.85	95/ 931.95
Stresses in the test positions, σ_i, MPa	I								
	II								
	III								
	IV								

As demonstrated in **Table 1**, the stresses increase in conjunction with the applied loads in all positions, thereby substantiating the anticipated linear correlation between load intensity and stress levels. The results demonstrate that the frame's design is capable of accommodating considerable stress without exceeding the permissible limits, particularly in Test Position IV, where the maximum load of 95 tons/MPa resulted in a stress level approaching the upper threshold. This serves to confirm the structural soundness of the hoist in the context of extreme conditions.

The calculations were performed for four test positions of the load-handling frame. Calculations were performed for 4 tested positions of the load-handling frame. Particular attention was paid to position 1, where the container has a tilt angle of 90° during loading. **Figure 1** depicts the calculation scheme employed to ascertain the static stresses within the load-handling frame of the stationary hoist. The diagram provides a visual representation of the model used in the mathematical analysis, illustrating the various forces acting on the frame and the corresponding stress points. The calculation scheme illustrated in **Figure 1** provides the basis for understanding the interaction between static forces and the frame during the loading process. By mapping out the forces and constraints, it becomes possible to predict the locations of potential stress points and to ensure that the structure can withstand the operational loads effectively.

Input data for the calculation are the following:

(i) length of a 20-foot container b = 6.037 m;
(ii) width of 20-foot container h = 2.5 m;
(iii) height of a 20-foot container l = 2.623 m;

DOI: http://dx.doi.org/10. 17509/xxxx.xxxx
p- ISSN 2776-6098 e- ISSN 2776-5938

(iv) diameter of grain cargo particles (wheat) d=0.4 cm;
(v) drop height of grain cargo h_0=7.037 m;
(vi) Determining the area of the hopper opening with a circular cross-section (see equation (1)):

$$S = \pi(0.01R)^2 = 0.071\ m^2, \quad (1)$$

where *R* is the hole radius;
(vii) Determining the area of the hopper opening with a rectangular cross-section (see equation (2)):

$$S = b_1^2 = 0.25\ m^2, \quad (2)$$

where b_1 = 0.5 m is the width of the track hopper with a rectangular opening.

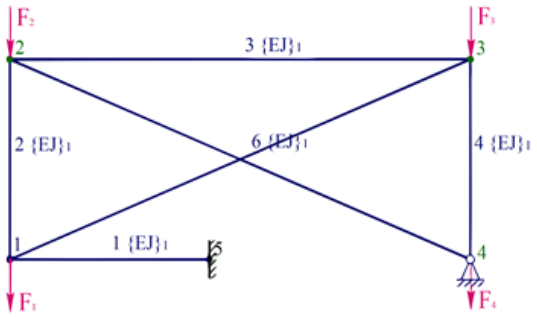

Figure 1. Calculation scheme for determining static stresses in the load-handling frame construction of a stationary hoist under development.

To determine the required radius of the downcomer pipes of the loading hopper, the radius was increased fourfold (i.e. 10, 15, 20, and 25 cm) according to the prescribed pitch of 5 cm (see **Table 2**). Calculations were carried out to determine the minimum container filling time and dynamic load at the tested position 1 (with the tilt angle of the container the 90°), with the implementation of four changes of the radius of the downcomer pipes of the loading hopper.

Table 2. Form for recording the obtained results.

Trials	1	2	3	4
Hole radius of the hopper opening, *R*, cm	10	15	20	25
Container filling time, t_V, min				
Dynamic stress, σ_d, MPa				

The data presented in **Table 2** illustrates that an increase in the radius of the downcomer pipes is accompanied by a notable reduction in the time required to fill the container. However, this increase in efficiency is accompanied by a corresponding rise in dynamic stresses, particularly when the hole radius reaches 25 cm. It is essential to exercise caution when optimizing the design of the loading hopper, as the trade-off between efficiency and stress must be carefully considered.

4. CONCLUSION

4.1. Results

The design scheme adopted for the calculation of static stresses in the construction of the load-handling frame of the stationary hoist under development is statically indeterminate because the right support is hinged immovable. The reaction X_b is determined by satisfying the compatibility of displacements. For this purpose, it is necessary to select the basic system,

DOI: http://dx.doi.org/10. 17509/xxxx.xxxx
p- ISSN 2776-6098 e- ISSN 2776-5938

which is statically determined. The load acting on the load-handling frame can be determined in equation (3):

$$P = m9.81 * 10 - 3\ kN, \quad (3)$$

where *m* is the mass of the container with grain cargo.

Figure 2 illustrates the spatial system employed in the calculation of the static and dynamic forces acting on the load-handling frame. This system considers the symmetrical distribution of forces and the impact of varying angles on the overall force distribution. To evaluate the stresses, the model accounts for both static equilibrium and dynamic influences, thus allowing for a more comprehensive analysis of the frame's structural integrity. The chosen spatial system of the calculation scheme for the load-handling frame is considered to be symmetrical. Thus, a planar fourfold statically indeterminate system is considered, where the force *F* is acting at an angle to the frame, and the angle α can vary from 0 to 90°. This example considers α = -0°= 0.

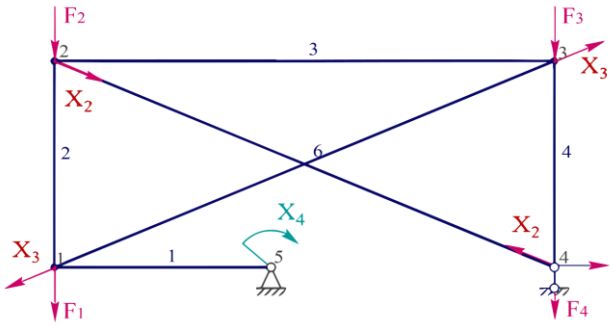

Figure 2. Spatial system.

The results presented in **Figure 2** underscore the importance of considering the influence of varying angles on the distribution of force. As the angle of inclination is increased, the force components shift, which in turn affects the stability and load-bearing capacity of the frame. The findings of this analysis indicate that optimizing the angle may result in a reduction in stress on critical sections, thereby enhancing the durability and performance of the hoist during loading operations.

For each of the 8 nodes of the spatial system, the force is determined (see equation (4)):

$$F = \frac{P}{8}. \quad (4)$$

This force is resolved into vertical and horizontal components (see equations (5) and (6)):

$$F_y = F * \cos(\alpha)\ kN, \quad (5)$$

$$F_x = F * \sin(\alpha)\ kN. \quad (6)$$

Referring to the beam in **Figure 3a** is the defined system. The level of static indeterminacy of this system is equal to one. By removing one of the links (of the right support), the basic system shown in **Figure 3b** is obtained, where the unknown reaction is denoted as *X*. There are several ways to eliminate redundant links, but not all of them are suitable for further calculation. For example, the scheme in **Figures 3c and 3f** is geometrically variable and is not suitable for calculation. The other schemes can be chosen as the basic system.

In linear elastic systems, the external load is uniformly distributed, which means that the calculation results should be the same for different basic systems. However, the capacity size

DOI: http://dx.doi.org/10. 17509/xxxx.xxxx
p- ISSN 2776-6098 e- ISSN 2776-5938

of computation may differ between the different basic systems. Thus, it is necessary to select the optimal basic system from multiple options. For example, in this case, the first variant of the basic system is preferable, because in it the diagrams are constructed more simply for a statically determined system, the solution is obtained by writing down the equations of equilibrium necessary to determine the reactions of the supports (see equation (7)):

$$\sum F_{ix} = 0, \sum F_{iy} = 0, \sum M_{F(.)} = 0 \quad (7)$$

Where F_X is the force on the *X*-axis, ΣF_{ix} is the sum of all forces on the *X*-axis; F_y is the force on the Y-axis, ΣF_{iy} is the sum of all forces on the Y-axis; $M_{F(B)}$ is the moment of force relative to point B, and $\Sigma M_{F(.)}$ is the sum of moments of forces?

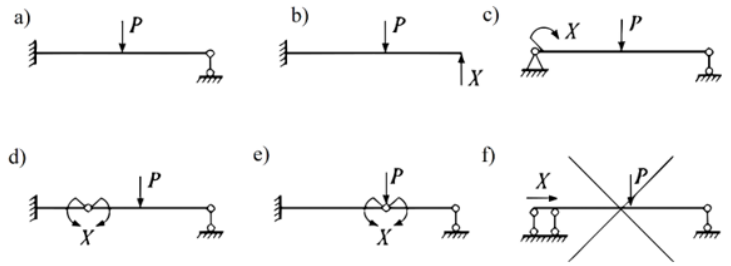

Figure 3. Options for the basic system: (a) Testing 1; (b) Testing 2, (c) Testing 3, (d) Testing 4, (e) Testing 5, and (f) Testing 6.

In the system, the angle α is changing. Any force can be resolved into two components using the parallelogram law: $F_y = F \cdot \cos(\alpha)$ and $F_x = F \cdot \sin(\alpha)$. Since forces (e.g., gravity) always point downwards, in this case, it is possible to rotate the forces rather than the load frame itself. Thus, the equations of equilibrium for the basic system will be drawn up (see equation (8)):

$$\sum M_A = 0{:}2F_y * l + Y_B(b - l) - 2F_y(b - l) + 2F_x h = 0, \quad (8)$$

where parameters of load-handling frame: *b* = 6.037 m; *h* = 2.5 m; *l* = 2.623 m. Thus, the bending moments diagram shown in **Figure 4** is obtained. Then, it reveals that the equilibrium condition is satisfied.

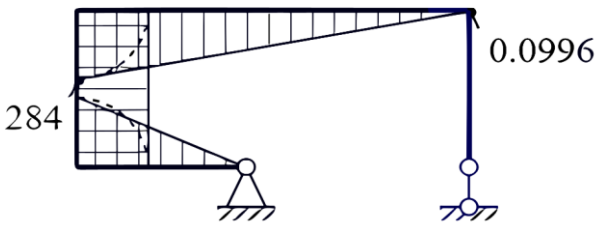

Figure 4. Bending moments diagram, Mx, kN*m.

The bending moments illustrated in **Figure 4** demonstrate that the maximum moments occur at specific points along the frame, particularly in areas where the forces are concentrated, such as the supports. These peaks indicate areas that may require reinforcement or design modifications to ensure stability. Furthermore, the gradual increase in the moment as the load intensifies indicates that elevated forces amplify strain in specific sections, which must be taken into account when designing frames for extended or substantial utilization. This analysis highlights the necessity of considering both static and dynamic conditions when determining the load-handling capacity of such systems.

DOI: http://dx.doi.org/10. 17509/xxxx.xxxx
p- ISSN 2776-6098 e- ISSN 2776-5938

The equation of moments is made sequentially, taking into account that if the force rotates anti-clockwise concerning a point, the moment will be positive, and vice versa (see equation (9)):

$$\Sigma M_B = 0{:}2F_y b - Y_A(b-1) + 2F_x h = 0. \quad (9)$$

Reactions support equations (10) and (11):

$$Y_B = \frac{2F_y(b-1) - 2F_y * 1 - 2F_x h}{b-1} = 14.206 \text{ kN}, \quad (10)$$

$$Y_A = \frac{2F_y b + 2F_x h}{b-1} = 108.419 \text{ kN}. \quad (11)$$

Since the algebraic sum of all forces directed along the *X*-axis is zero, hence equation (12) becomes:

$$\Sigma F_{xi} = X_A - 4F_x = 0, X_A = 4F_x = 0 \text{ kN}, Y_A + Y_B - 4F_y = 0 \quad (12)$$

Where X_A and Y_A are the reactions of supports in joint A; X_B and Y_B are the reactions of supports in joint B.

Although the calculation is carried out in bending and the bending moments are basic to the calculation, allow for the effect of longitudinal forces in this calculation, as there is an internal frame circuit operating in the tension-compression (see equation (13)):

$$N_{1F}(z) = X_A, \quad (13)$$

where *N* is the longitudinal force, which acts in compression (-) or tension (+); *Q* is the transverse force.

If the beam is shown as a material, then the force that is directed along the axis is *N*, the perpendicular force is *Q*, and there is a bending moment *M*. Then, equation (14) becomes

$$N_{2F}(z) = F_y - Y_A;$$

$$N_{3F}(z) = F_x - X_A;$$

$$N_{4F}(z) = F_y - Y_B;$$

$$N_{5F}(z) = 0;$$

$$N_{6F}(z) = 0;$$

$$Q_{1F} = -Y_A = -108.419 \text{ kN};$$

$$Q_{2F} = F_x = 0;$$

$$Q_{3F} = Y_A - 2F_y = 47.107 \text{ kN};$$

$$Q_{4F} = F_x = 0;$$

$$M_{1F}(z) = -Y_A z; M_{1F}(0) = 0; \quad (14)$$

$$M_{1F}(1) = -284.384 \text{ kNm};$$

$$M_{2F}(z) = -Y_A * 1 - X_A z + F_x z;$$

$$M_{2F}(0) = -284.384 \text{ kNm};$$

$$M_{2F}(h) = -284.384 \text{ kNm};$$

DOI: http://dx.doi.org/10. 17509/xxxx.xxxx
p- ISSN 2776-6098 e- ISSN 2776-5938

$$M_{3F}(z) = -Y_A(1-z) - 2F_y z + F_x h - X_A h;$$

$$M_{3F}(0) = -284.384 \text{ kNm};$$

$$M_{3F}(b) = 0;$$

$$M_{4F}(z) = -F_x(h-z);$$

$$M_{4F}(0) = 0;$$

$$M_{4F}(h) = 0.$$

Figure 5a illustrates the internal force factor distribution resulting from the application of unit forces to the frame. The role of internal forces in the overall stability of the structure is of considerable importance, as they represent how the frame itself responds to external forces. **Figure 5b** elucidates the intricate dynamics of force interactions within the frame, illustrating how the internal components respond to stress, tension, and compression during the loading process. Then a unit system is defined, which is the same basic system, but with unit forces applied to it. Instead of immovable support, a force equal to one is substituted in equation (15):

$$X = 1; X_x = 1;$$

$$X_{1a} = -X_x = -1;$$

$$X_y = 0;$$

$$Y_{1b} = X_y = 0;$$

$$Y_{1a} = 0;$$

$$N_{11}(z) = X_{1a};$$

$$N_{12}(z) = 0;$$

$$N_{13}(z) = -X_{1a};$$

$$N_{14}(z) = 0;$$

$$N_{15}(z) = 0;$$

$$N_{16}(z) = 0;$$

$$M_{11}(z) = 0; \quad (15)$$

$$M_{12}(z) = (-X_{1a})\, z;$$

$$M_{12}(0) = 0;$$

$$M_{12}(h) = 2.5 \text{ kNm};$$

$$M_{13}(z) = -X_{1a}\, h;$$

$$M_{13}(0) = 2.5 \text{ kNm};$$

$$M_{13}(b) = 2.5 \text{ kNm};$$

$$M_{14}(z) = X_x\, (h-z);$$

$$M_{14}(0) = 2.5 \text{ kNm};$$

DOI: http://dx.doi.org/10. 17509/xxxx.xxxx
p- ISSN 2776-6098 e- ISSN 2776-5938

$$M_{14}(h) = 0.$$

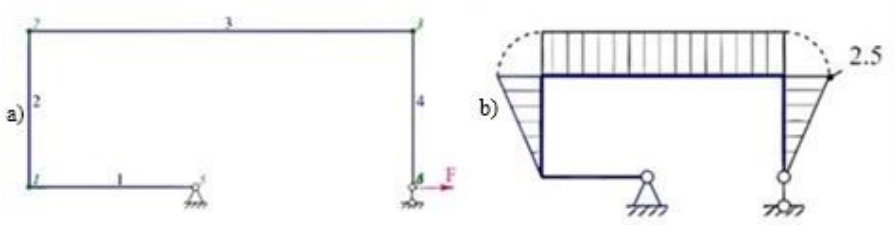

Figure 5. Configuration of the basic system with applied unit force (a) and corresponding internal force factor diagrams (b).

The static indeterminacy can be solved using the force method. In this case, there are four unknown reactions. Thus, the same number of equations will be generated using the force method equation (16):

$$\beta = \operatorname{atan}\left(\frac{h}{b}\right) = 0.393,$$

$$X_{2x} = X\cos(\beta) = 0.924, \tag{16}$$

$$X_{2y} = X\sin(\beta) = 0.383,$$

$$\beta = 22.495\text{deg}.$$

The influence of the unit forces of the inner circuit is shown in **Figure 6**.

Figure 6a shows the distribution of unit forces (X_2) within the inner circuit, emphasizing areas where these forces are applied. This distribution serves to demonstrate how unit forces contribute to stress across various points within the structure. **Figure 6b** shows the variation of bending moments under these unit forces. This diagram shows areas of high concentration, highlighting areas more susceptible to stress and potential failure under large or repetitive loads. Influence of unit forces of the inner circuit (see equation (17)):

$$X_{2x}\,h - X_{2y}\,1 + Y_{2b}(b-1) - X_{2y}\,(b-1) = 0,$$

$$-X_{2y}\,b + X_{2x}\,h - Y_{2a}(b-1) = 0,$$

$$X_{2a} = 0,$$

$$X_{2y} - X_{2y} + Y_{2a} + Y_{2b} = 0, \tag{17}$$

$$Y_{2b} = \frac{X_{2y}b - X_{2x}h}{b-l} = 0,$$

$$Y_{2a} = \frac{X_{2x}h - X_{2y}b}{b-l} = 0.$$

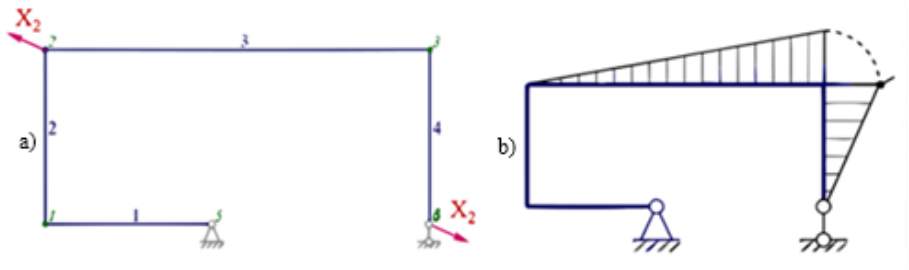

Figure 6. Influence of unit forces (X_2) in the inner circuit (a) and bending moments diagram resulting from their action (b)

DOI: http://dx.doi.org/10. 17509/xxxx.xxxx
p- ISSN 2776-6098 e- ISSN 2776-5938

Determination of unit forces concerns the X and Y axes, as shown in equations (18), (19), and (20):

$$X_{3x} = X\cos(\beta) = 0.924,$$
$$X_{3y} = X\sin(\beta) = 0.383,$$
$$X_{3y}\,1 + X_{3y}\,(b-1) + Y_{3b}(b-1) - X_{3x}\,h = 0, \quad (18)$$
$$X_{3y}\,b - X_{3x}\,h - Y_{2a}(b-1) = 0,$$
$$X_{3a} = 0.$$

$$Y_{3a} + Y_{3b} - X_{3y} + X_{3y} = 0,$$
$$Y_{3b} = \frac{X_{3y}b - X_{3x}h}{b-l} = 0, \quad (19)$$
$$Y_{3a} = \frac{X_{3y}b - X_{3x}h}{b-l} = 0.$$

$$N_{21}(z) = 0,$$
$$N_{22}(z) = 0,$$
$$N_{23}(z) = X_{2x},$$
$$N_{24}(z) = X_{2y},$$
$$N_{25}(z) = X,$$
$$N_{26}(z) = 0,$$
$$N_{31}(z) = 0,$$
$$N_{32}(z) = 0,$$
$$N_{33}(z) = X_{2x},$$
$$N_{34}(z) = X_{2y},$$
$$N_{35}(z) = X,$$
$$N_{36}(z) = 0,$$
$$M_{21}(z) = 0,$$
$$M_{22}(z) = 0, \quad (20)$$
$$M_{23}(z) = X_{2y}\,z,$$
$$M_{24}(z) = X_{2x}\,(h-z),$$
$$M_{22}(0) = 0,$$
$$M_{23}(0) = 0,$$
$$M_{24}(0) = 2.31\ \text{kNm},$$

DOI: http://dx.doi.org/10. 17509/xxxx.xxxx
p- ISSN 2776-6098 e- ISSN 2776-5938

$$M_{22}(h) = 0,$$

$$M_{23}(b) = 2.31\ \text{kNm},$$

$$M_{24}(h) = 0,$$

$$M_{31}(z) = 0,$$

$$M_{32}(z) = X_{3x}\, z,$$

$$M_{33}(z) = X_{3x}\, h - X_{3y}\, z,$$

$$M_{34}(z) = 0,$$

$$M_{32}(0) = 0,$$

$$M_{33}(0) = 2.31\ \text{kNm},$$

$$M_{34}(0) = 0,$$

$$M_{32}(h) = 2.31\ \text{kNm},$$

$$M_{33}(b) = 0,$$

$$M_{34}(h) = 0.$$

Thus, the bending moments diagram from the unit forces (X_3) of the inner circuit, shown in **Figure 7**, is obtained. This figure provides a more detailed examination of the localized effects of unit forces and their impact on specific areas of the frame. The objective is to investigate how localized stress can result in structural deformation or failure.

Figure 7a displays the distribution of unit forces (X_3) within the inner circuit, illustrating how these forces interact with the frame and pinpointing areas where the force concentration is most significant Figure 7b shows the resulting bending moments diagram, which highlights the concentrated stress points created by the action of the unit forces (X_3). These concentrated bending moments suggest areas vulnerable to material fatigue or failure if not reinforced properly. The bending moments are defined as follows in equations (21) and (22):

$$\Sigma M_A = X_4 + X_{4b}\,(b-1) = 0, \tag{21}$$

$$\Sigma M_B = X_4 + X_{4a}\,(b-1) = 0. \tag{22}$$

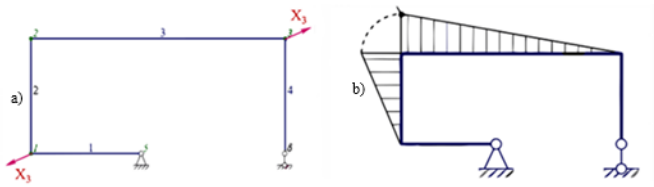

Figure 7. Influence of unit forces (X_3) of the inner circuit (a) and bending moments diagram from their action (b).

The reactions of the supports are determined from the equilibrium conditions (see equation (23)):

$$Y_{4b} = \frac{-X_4}{b-1} = -0.293,\ Y_{4a} = \frac{X_4}{b-1} = 0.29. \tag{23}$$

The internal force factors for a given system in each section are determined (see equation (24)):

DOI: http://dx.doi.org/10. 17509/xxxx.xxxx
p- ISSN 2776-6098 e- ISSN 2776-5938

$$N_{41}(z) = 0,$$

$$N_{42}(z) = -Y_{4a},$$

$$N_{43}(z) = 0,$$

$$N_{44}(z) = -Y_{4b},$$

$$N_{45}(z) = 0,$$

$$N_{46}(z) = 0, \quad (24)$$

$$M_{41}(z) = -X_4 - Y_{4a}z,$$

$$M_{41}(0) = -1,$$

$$M_{41}(1) = -1.768\ \text{kNm},$$

$$M_{42}(z) = -X_4 - Y_{4a} * 1,$$

$$M_{42}(h) = -1.768\ \text{kNm},$$

$$M_{43}(z) = -X_4 - Y_{4a}(1 - z).$$

Based on the results of the calculation, the diagrams were constructed and presented in **Figure 8**.

Figure 8a illustrates the applied unit moment at the left support, showing how the forces are distributed around this critical area. This emphasizes that the left support is the primary area experiencing significant bending moments. **Figure 8b** highlights the areas where bending moments are most concentrated, signaling regions that may require additional reinforcement. The condition under which the displacement along the i-th bond of the n discarded bonds is zero is determined by the principle of independence of forces and is expressed in equation (25):

$$\Delta_i = \Delta_{i1} + \Delta_{i2} + \cdots + \Delta_{in} + \Delta_{iF} = 0. \quad (25)$$

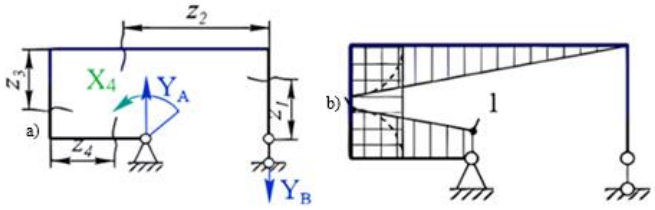

Figure 8. The bending moments diagram of action unit moment (a) action on the left support (b), $X_4 = 1$.

Here, the first index indicates the direction of movement and the number of discarded bonds, and the second index indicates the cause that triggered the movement. Δ_{ik} represents the movement along the i-th bond caused by the reaction of the kth bond. Δ_{ik} represents the displacement along the i-th bond that occurs as a result of the simultaneous effect of the entire external load. In the force method, the reaction on the k-th bond is denoted as x_k. Using Hooke's law, the displacements Δ_{ik} can be expressed in equation (26):

$$\Delta_{ik} = \delta_{ik} x_k, \quad (26)$$

where δ_{ik} is the unit displacement along the i-th bond that occurs as a result of the reaction $\bar{x}_k = 1$, Which has the same direction as x_k, But its magnitude is one.

DOI: http://dx.doi.org/10. 17509/xxxx.xxxx
p- ISSN 2776-6098 e- ISSN 2776-5938

Using equations (25) and (26), the following results are obtained (see equation (27)):

$$\Delta_i = \delta_{i1}x_1 + \delta_{i2}x_2 + \cdots + \delta_{in}x_n + \Delta_{iF} = 0. \quad (27)$$

Equation (27) expresses the physical meaning that the displacement on the i-th discarded bond in the basic system is zero (see equation (28)):

$$\left\{\begin{array}{l} \mathrm{x_1\delta_{i1} + x_2\delta_{i2} + \cdots + x_n\delta_{in} + \Delta_{ip} = 0} \\ \mathrm{x_1\delta_{21} + x_2\delta_{22} + \cdots + x_n\delta_{2n} + \Delta_{2p} = 0} \\ \mathrm{\ldots\ldots\ldots\ldots\ldots\ldots\ldots\ldots\ldots\ldots\ldots\ldots\ldots\ldots\ldots\ldots} \\ \mathrm{x_1\delta_{1n} + x_2\delta_{2n} + \cdots + x_n\delta_{nn} + \Delta_{np} = 0} \end{array}\right\}. \quad (28)$$

where $\delta_{ik} = \int \frac{\bar{M}_i \bar{M}_k}{El} dx$ is the unit coefficients (displacements); $\bar{M}_i \bar{M}_k$ is the moments from unit forces applied in the direction of unknown $x_{i,} x_k$; *El* is the bending stiffness. Generalized displacements $\Delta_{ip} = \int \frac{\bar{M}_i M_p}{El} dx$ is the called load coefficients (displacements); $\bar{M}_i$ is the bending moment caused by the i-th unit force; M_p denotes the bending moment that arises as a result of a system of external forces.

The coefficients of the canonical equation using the force method are determined, and the transient stiffness coefficients of the system are written. Inertia ratio (29):

$$\frac{\mathrm{I_{xD}}}{\mathrm{I_{xS}}} = 2.199. \quad (29)$$

The transient coefficients of reduced stiffness are calculated for the I-beam, channel and angles of the inner circuit of the frame. Cross-section area of the I-beam (see equation (30)):

$$\mathrm{A_D} = 225 * 10^{-4} = 0.023,$$

$$\mu = \frac{\mathrm{I_{xD}}}{\mathrm{A_D}} = 0.014,$$

$$\mathrm{v} = \frac{\mathrm{I_{xD}}}{\frac{\mathrm{A_D}}{2}} = 0.029, \quad (30)$$

$$\xi = \frac{\mathrm{I_{xD}}}{\mathrm{A_D} * 0.2} = 0.072,$$

where *k* = 2.199 is the inertia ratio ($\frac{\mathrm{I_{xD}}}{\mathrm{I_{xS}}}$); μ = 0.014 is the transient coefficient of reduced stiffness for the I-beam; *v* = 0.029 is the same for the channel; ξ = 0.072 is the same for the angles.

Mora's method is used to calculate unit and load displacements in the canonical equations (31) and (32):

$$\delta_{ik} = \int \frac{\bar{M}_i \bar{M}_k}{El} dx, \quad (31)$$

$$\Delta_{ip} = \int \frac{\bar{M}_i M_p}{El} dx. \quad (32)$$

The process of deriving a universal equation for determining the deflection at point K of a simply supported beam in bending will be discussed. **Figure 9** shows a simply supported beam without load at point *K*. To find the deflection at point *K*, the auxiliary state of the beam is considered when a force *T* is applied at point *K*. This state is called a fictitious state because it is not physical, but it is necessary for displacement calculations. First, the work of external forces and the strain energy for a given auxiliary state are determined. The force *T* that causes

DOI: http://dx.doi.org/10. 17509/xxxx.xxxx
p- ISSN 2776-6098 e- ISSN 2776-5938

the displacement Δ_{KT} at point K is calculated. For this purpose, Clapeyron's theorem is used in equation (33) (Barbieri and Botto, 2021):

$$A_T = \frac{1}{2} T \Delta_{\mathrm{KT}}. \tag{33}$$

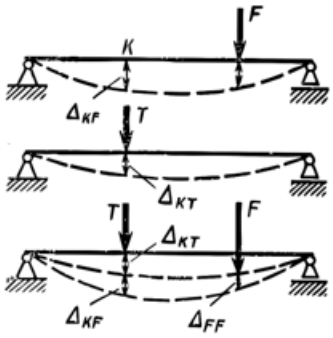

Figure 9. Scheme of a simply supported beam.

The internal force factors depicted in **Figure 9** indicate that load distribution varies significantly depending on the position and magnitude of the applied forces. The data indicate that specific areas of the frame are subjected to disproportionately high loads, which could potentially result in fatigue or failure over time. Mitigation of these risks may be achieved by reinforcing the high-stress zones or redistributing the load more evenly, thus ensuring that the frame maintains its structural integrity throughout its operational life.

The corresponding strain energy is shown in equation (34):

$$\mathrm{U_T} = \sum \int_{\mathrm{l_i}} \frac{\mathrm{M_{xT}^2 dz}}{\mathrm{2EJ_x}}, \tag{34}$$

Where M_{xT} is the bending moment in an arbitrary cross-section of the beam caused by the force T. Consequently, A_T = U_T can describe equation (35):

$$\frac{1}{2}\mathrm{T\Delta_{KT}} = \sum \int_{\mathrm{l_i}} \frac{\mathrm{M_{xT}^2 dz}}{\mathrm{2EJ_x}}. \tag{35}$$

Supposing that on an already loaded beam, which is subjected to a force *T*, an additional force *P* is applied at point *K*. As a result, an additional displacement Δ_{KP} occurs at point *K*, and force *T* does additional work (see equation (36)):

$$\mathrm{A_{TP}} = \mathrm{T\Delta_{KP}}. \tag{36}$$

In the equations for work and energies provided above, the coefficient ½ is missing. This is because when force *P* is applied to a beam with already applied force *T*, the value of force *T* does not change. In this case, the force *P* does the work when moving the point of application Δ_{PP} (see equation (37)):

$$\mathrm{A_P} = \frac{1}{2}\mathrm{P\Delta_{PP}}. \tag{37}$$

The equation for calculating the strain energy related to loading the beam with force *P* is is shown in equation (38):

$$\mathrm{U_P} = \sum \int_{\mathrm{l_i}} \frac{\mathrm{M_{xP}^2 dz}}{\mathrm{2EJ_x}}. \tag{38}$$

Consequently, in this case, $A_P = U_P$ is in equation (39):

DOI: http://dx.doi.org/10. 17509/xxxx.xxxx
p- ISSN 2776-6098 e- ISSN 2776-5938

$$\frac{1}{2}P\Delta_{PP} = \sum\int_{l_i}\frac{M_{xP}^2 dz}{2EJ_x}. \quad (39)$$

The total work done by external forces can be expressed as the sum of three summands (see equation (40)):

$$A = A_T + A_P + A_{TP} = \frac{1}{2}T\Delta_{KT} + \frac{1}{2}P\Delta_{PP} + T\Delta_{KP}. \quad (40)$$

To determine the deformation energy in the bending of a beam subjected to the action of forces *T* and *P* simultaneously, taking into account that $M_x = M_{xT} + M_{xP}$ (The principle of independent force action is used to calculate bending moments) (see equation (41)):

$$U = \sum\int_{l_i}\frac{(M_{xT}+M_{xP})^2}{2EJ_x}dz. \quad (41)$$

Expanding the parentheses obtained equation (42):

$$U_P = \sum\int_{l_i}\frac{M_{xT}^2 dz}{2EJ_x} + \sum\int_{l_i}\frac{M_{xP}^2 dz}{2EJ_x} + \sum\int_{l_i}\frac{M_{xP}M_{xT}dz}{2EJ_x}. \quad (42)$$

Equating the right-hand sides of expressions, we obtained equation (43):

$$\frac{1}{2}T\Delta_{KT} + \frac{1}{2}P\Delta_{PP} + T\Delta_{KP} = \sum\int_{l_i}\frac{M_{xT}^2 dz}{2EJ_x} + \sum\int_{l_i}\frac{M_{xP}^2 dz}{2EJ_x} + \sum\int_{l_i}\frac{M_{xP}M_{xT}dz}{2EJ_x}. \quad (43)$$

Considering that the left-hand sides of the first and second equations are equal to the first and second sums of the integrals in the right-hand side, respectively (equations (35) and (39)), then it is possible to obtain equation (44):

$$T\Delta_{KP} = \sum\int_{l_i}\frac{M_{xP}M_{xT}dz}{EJ_x}. \quad (44)$$

To determine the desired displacement (Δ_{KP}), divide both parts of the resulting expression by T, then we obtain equation (45):

$$\Delta_{KP} = \sum\int_{l_i}\frac{M_{xP}\frac{M_{xT}}{T}dz}{EJ_x}. \quad (45)$$

The quantity $\frac{M_{xT}}{T}$ has the dimension of length. This refers to the unit moment, which represents the bending moment in an arbitrary beam cross-section caused by the action of a dimensionless force with unit quantity applied at the point where the displacement is to be determined. M_1 represents this moment and is used for convenience in the equations. Mora's equation is expressed in the following form (see equation (46)):

$$\Delta_{KP} = \sum\int_{l_i}\frac{M_P M_1 dz}{EJ_x}. \quad (46)$$

If consider both bending moments and transverse forces, then the equation for the Mora's integral takes the following form (see equation (47)):

$$\Delta_{KP} = \sum\int_{l_i}\frac{M_P M_1 dz}{EJ_x} + \sum\int_{l_i}\frac{kQ_P Q_1 dz}{GF}, \quad (47)$$

where Q_p and Q_1 is the expressions for the transverse forces due to the given load and unit force, obtained for an arbitrary cross-section of the beam. Determination of displacement due to the action of central forces can obtain equation (48):

DOI: http://dx.doi.org/10. 17509/xxxx.xxxx
p- ISSN 2776-6098 e- ISSN 2776-5938

$$\delta_{N1F} = \mu * \int_0^1 N_{1F}(z) * N_{11}(z)dz + v * \int_0^h N_{2F}(z) * N_{12}(z)dz + \mu * \int_0^b N_{3F}(z) * N_{13}(z)dz + v * \int_0^h N_{4F}(z) * N_{14}(z)dz + \xi * \int_0^{\frac{b}{\cos(\beta)}} N_{5F}(z) * N_{15}(z)dz + \xi * \int_0^{\frac{b}{\cos(\beta)}} N_{6F}(z) * N_{16}(z)dz = 0, \quad (48)$$

where δ is the force displacement. By analogy, the coefficients of the canonical equations for the other sections of the frame are determined ($\delta_{N2F}, \delta_{N3F}, \delta_{N4F}$). In order to find δ the Mora's integral, is used to determine the deformations or displacements in bending using this dependence of moments (see equation (49)):

$$\Delta_{1F} = \int_0^1 M_{1F}(z) * M_{11}(z)dz + k * \int_0^h M_{2F}(z) * M_{12}(z)dz + \int_0^b M_{3F}(z) * M_{13}(z)dz + k * \int_0^h M_{4F}(z) * M_{14}(z)dz + \delta_{N1F} = -4.1 * 10^3. \quad (49)$$

Similarly, $\Delta_{2F}, \Delta_{3F}, \Delta_{4F}$ are determined (see equations (50) and (51)):

$$\delta_{N11} = \mu * \int_0^1 N_{11}(z)^2dz + v * \int_0^h N_{12}(z)^2dz + \mu * \int_0^b N_{13}(z)^2dz + v * \int_0^h N_{14}(z)^2dz + \xi * \int_0^{\frac{b}{\cos(\beta)}} N_{15}(z)^2dz + \xi * \int_0^{\frac{b}{\cos(\beta)}} N_{16}(z)^2dz = 0.121, \quad (50)$$

$$\delta_{11} = \int_0^1 M_{11}(z) * M_{11}(z)dz + k * \int_0^h M_{12}(z) * M_{12}(z)dz + \int_0^b M_{13}(z) * M_{13}(z)dz + k * \int_0^h M_{14}(z) * M_{14}(z)dz + \delta_{N11} = 60.759. \quad (51)$$

Similarly, $\delta_{N22}, \delta_{22}, \delta_{N33}, \delta_{33}, \delta_{N44}, \delta_{44}, \delta_{N12}, \delta_{12}, \delta_{N13}, \delta_{13}, \delta_{N23}, \delta_{23}, \delta_{N14}, \delta_{14}, \delta_{N24}, \delta_{24}, \delta_{N34}, \delta_{34}$ are determined (see equation (52) and (53)):

$$B = \begin{bmatrix} \delta_{11} & \delta_{12} & \delta_{13} & \delta_{14} \\ \delta_{12} & \delta_{22} & \delta_{23} & \delta_{24} \\ \delta_{13} & \delta_{23} & \delta_{33} & \delta_{34} \\ \delta_{14} & \delta_{24} & \delta_{34} & \delta_{44} \end{bmatrix} = \begin{bmatrix} 60.759 & 28.09 & 28.09 & -25.496 \\ 28.09 & 21.066 & 5.921 & -4.101 \\ 28.09 & 5.921 & 21.066 & -19.438 \\ -25.496 & -4.101 & -19.438 & 28.649 \end{bmatrix} \quad (52)$$

$$D = \begin{pmatrix} -\Delta_{1F} \\ -\Delta_{2F} \\ -\Delta_{3F} \\ -\Delta_{4F} \end{pmatrix} = \begin{pmatrix} 4.1 \times 10^3 \\ 660.459 \\ 3.127 \times 10^3 \\ -4.343 \times 10^3 \end{pmatrix}. \quad (53)$$

Solving the system of canonical equations by matrix method, the unknown reactions of the system (see equation (54)) are determined:

$$x = \begin{pmatrix} 10.551 \\ -12.777 \\ 13.563 \\ -134.813 \end{pmatrix}. \quad (54)$$

Verification of the solution of the system obtains equation (55):

$$\begin{aligned} \delta_{11}x_1 + \delta_{12}x_2 + \delta_{13}x_3 + \delta_{14}x_4 &= 4.1 * 10^3, \\ \delta_{12}x_1 + \delta_{22}x_2 + \delta_{23}x_3 + \delta_{24}x_4 &= 660.459, \\ \delta_{13}x_1 + \delta_{23}x_2 + \delta_{33}x_3 + \delta_{43}x_4 &= 3.127 * 10^3, \\ \delta_{14}x_1 + \delta_{24}x_2 + \delta_{34}x_3 + \delta_{44}x_4 &= -4.343 * 10^3. \end{aligned} \quad (55)$$

In order to construct the final internal force-factor diagrams, it is necessary to preliminarily (sometimes not always) calculate the support reactions for this equivalent system using the equilibrium conditions (see equations (56)-(61)):

DOI: http://dx.doi.org/10. 17509/xxxx.xxxx
p- ISSN 2776-6098 e- ISSN 2776-5938

$$X_b = x_1 = 10.551,$$

$$X_1 = x_2 = -12.777,$$

$$X_2 = x_3 = 13.563,$$

$$\beta = 22.495\text{deg},$$

$$X_4 = x_4,$$

$$X_{1x} = X_1 \cos(\beta) = -11.805, \tag{56}$$

$$X_{2x} = X_2 \cos(\beta) = 12.531,$$

$$X_{1y} = X_1 \sin(\beta) = -4.889,$$

$$X_{2y} = X_2 \sin(\beta) = 5.189,$$

$$X_a + X_b - 4F_x = 0,$$

$$X_a = 4F_x - X_b = -10.551 \text{ kN}.$$

$$2F_y * 1 + Y_b\,(b-1) - 2F_y(b-1) + 2F_x\,h + X_{1x}\,h - X_{1y}1 - X_{1y}(b-1) + X_{2y}(b-1) - X_{2x}\,h + X_{2y} * 1 + X_4 = 0. \tag{57}$$

$$Y_b = -\frac{2F_x\,h - 2F_y\,b + 4F_y * 1 - X_{1y}b + X_{2y}b + X_{1x}h - X_{2x}h + X_4}{b-1} = 53.694 \text{ kN}. \tag{58}$$

$$2F_y\,b - Y_a\,(b-1) + 2F_x h + X_{1x}\,h - X_{1y}\,b + X_{2y}b - X_{2x}h + X_4 = 0. \tag{59}$$

$$Y_a = \frac{2F_y\,b + 2F_x\,h - X_{1y}b + X_{2y}b + X_{1x}h - X_{2x}h + X_4}{b-1} = 68.931 \text{ kN}. \tag{60}$$

$$Y_a + Y_b - 4F_y = 0. \tag{61}$$

Determination of internal force factors for the equivalent system (see equation (62)):

$$N_1 = X_a = -10.551 \text{ kN},$$

$$N_2 = -Y_a + F + X_2 \sin(\beta) = -33.086,$$

$$N_3 = -X_a + X_2 \cos(\beta) + X_1 \cos(\beta) = 11.277,$$

$$N_4 = -Y_b + F + X_1 \sin(\beta) = -27.926 \text{ kN},$$

$$M_1(z) = -Y_a z - X_4,$$

$$M_1(0) = 134.813 \text{ kNm},$$

$$M_1(1) = -45.994 \text{ kNm},$$

$$M_2(z) = -Y_a * 1 - X_a z + F_x z + X_{2x} z - X_4,$$

$$M_2(0) = -45.994 \text{ kNm}, \tag{62}$$

$$M_2(h) = 11.711 \text{ kNm},$$

$$M_3(z) = -Y_a\,(1-z) - 2F_y z + F_x h - X_a h + X_{2x} h - X_{2y} z + X_{1y} z - X_4,$$

$$M_3(0) = 11.711 \text{ kNm},$$

$$M_3(b) = -3.134 \text{ kNm},$$

DOI: http://dx.doi.org/10. 17509/xxxx.xxxx
p- ISSN 2776-6098 e- ISSN 2776-5938

$$M_4(z) = -F_x\,(h - z) + X_b(h - z) + X_{1x}(h - z),$$

$$M_4(0) = -3.134\ \text{kNm},$$

$$M_4(h) = 0\ \text{kNm},$$

$$M_{max} = \max(|M_1(0)|, |M_2(h)|, |M_3(b0)|, |M_4(h)|) = 134.813\ \text{kNm}.$$

The largest longitudinal force obtains equation (63):

$$N_{max} = \max(|N_1|, |N_2|, |N_3|, |N_4|) = 33.086\ \text{kN}. \quad (63)$$

The largest value of the moment is determined: maximum moment: M_{max} = 134.13 kN. **Figure 10a** shows the internal force coefficient diagram for one particular loading scenario, emphasizing the distribution and magnitude of internal forces throughout the frame. This gives an indication of areas of higher stress, especially near the supports. **Figure 10b** shows an internal force factor diagram for an alternative or combined loading scenario, offering a comparative view of the force distribution and further illustrating the stress concentration in the frame.

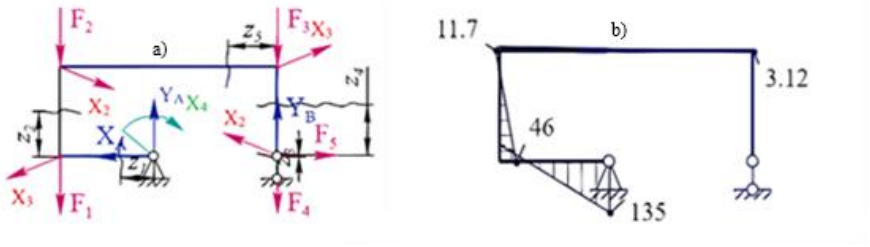

Figure 10. Final configuration of the internal force factors (a) and corresponding diagrams of internal force distributions (b)

The final force factor in **Figure 10** corroborates the hypothesis that specific areas of the frame, particularly those in proximity to the supports, are subjected to the greatest stress. This highlights the necessity for targeted reinforcement in these areas, in order to guarantee that the frame is capable of withstanding both static and dynamic loads in an efficient manner. Furthermore, the diagrams illustrate that while certain sections of the frame are capable of withstanding the loads applied, others are more susceptible and may necessitate additional consideration during the design phase to guarantee long-term stability. I-beam (strength test) (see equations (64) and (65)):

$$I_{xD} = 32344 * 10^{-8}\ \text{m}, \quad (64)$$

where y_{max} = 15 sm (the most distant point from the centre of the cross-section in the I-beam); I is the moment of inertia; W is the moment of resistance; $|\sigma|$ = 160 MPa (allowable tension). Then, we can get equation (65):

$$W_{xD} = \frac{I_{xD}}{y_{max} * 10^{-2}} = 2.156 * 10^{-3}\ \text{m}^3,$$

$$E = 2 * 10^8,$$

$$A_D = 225 * 10^{-4},$$

$$E \cdot I_{xD} = 6.469 * 10^4, \quad (65)$$

$$\left(\sigma_{max} = \frac{|M_{max}|}{W_{xD}}\right) \le |\sigma|,$$

DOI: http://dx.doi.org/10. 17509/xxxx.xxxx
p- ISSN 2776-6098 e- ISSN 2776-5938

$$\sigma = \frac{|N_1|*10^{-3}}{A_D} + \frac{M_{max}*10^{-3}}{W_{xD}} = 62.99 \text{ MPa}.$$

Channel (strength test) obtains equation (66):

$$I_{xS} = 14709 * 10^{-8} \text{ m}^4,$$

$$EI_{xS} = 2.942 * 10^4,$$

$$W_{xS} = \frac{I_{xS}}{y_{max}*10^{-2}} = 9.806 * 10^{-4} \text{ m}^3, \quad (66)$$

$$\sigma = \frac{M_{max}\cdot 10^3}{W_{xS}} * 10^{-6} = 137.48 \text{ MPa}.$$

Table 3 contains the results of the calculation of static stresses in the structure of the load-handling frame of the stationary hoist under development, obtained using the MathCad software environment.

Table 3. Results of static stress calculation performed in MathCad application program

Trials		**1**	**2**	**3**	**4**	**5**	**6**	**7**	**8**
Loadings to the structure, m_i, t/MPa		25/ 245.25	35/ 343.35	45/ 441.45	55/ 539.55	65/ 637.65	75/ 735.75	85/ 833.85	95/ 931.9
Stresses in the test positions, σ_i, MPa	I	28.34	39.67	51	62.34	73.67	85	96.34	107.7
	II	11.26	15.77	20.28	24.78	29.29	33.8	38.3	42.81
	III	42.87	60.02	77.17	94.32	111.5	128.6	145.8	162.9
	IV	62.99	88.2	113.4	138.6	163.8	188.9	214.2	239.4

Theoretical studies performed in the MathCad software environment showed that the obtained maximum stresses occur in position 4 of test No. 8 is the 239.363 MPa, and do not exceed the permissible stress is the 250 MPa. Thus, the obtained values of maximum normal stresses in the construction of the load-handling frame of the developed stationary hoist (**Table 3**) fully satisfy the condition of strength, i.e., the maximum stresses do not exceed the permissible stresses. Modeling of the process of filling the container with grain cargoes begins with determining the length and width of the rectangular opening of the downcomer pipes of the loading hopper (see equation (67)):

$$a_1 = \frac{S}{b_1} = 0.141 \text{ m}. \quad (67)$$

Lukyanov's equation for calculating the flow rate of bulk media is used to get equations (68) and (69):

$$V_1 = 0.344\sqrt{R}\frac{(R^2 - 1.9dR + 1.66d^2)}{3600} = 0.079 \text{ m/s}. \quad (68)$$

$$V_1 = b_1 a_1^{1.5}\sqrt{9.81} = 0.083 \text{ m}^3/\text{s}. \quad (69)$$

The initial velocity of falling particles obtains equation (70):

$$v_0 = \sqrt{9.81 a_1} = 1.178 \text{ m}^3/\text{s}. \quad (70)$$

Raw material consumption (wheat): V = 0.083 m^3/s; and Wheat density: ρ = 811 kg/m^3. Determination of mass flow rate of raw material (wheat) obtains equation (71):

DOI: http://dx.doi.org/10. 17509/xxxx.xxxx
p- ISSN 2776-6098 e- ISSN 2776-5938

$$m_0 = \rho V = 67.51 \text{ kg/s}. \quad (71)$$

Falling height of bulk medium (wheat) obtains equation (72):

$$h_0 = b + 1 = 7.037 \text{ m}. \quad (72)$$

Time of falling of particles obtains equation (73):

$$t = \sqrt{\frac{2h_0}{9.81}} = 1.198 \text{ s}. \quad (73)$$

Mass of the falling medium (wheat) obtains equation (74):

$$m=m_0*t=80.862 \text{ kg}. \quad (74)$$

Final velocity obtains equation (75):

$$v = \sqrt{v_0^2 + 2 * 9.81 * h_0} = 11.809. \quad (75)$$

Time to fill a twenty-foot container obtains equation (76):

$$t_V = \frac{2bh}{V60} = 6.044 \text{ min}. \quad (76)$$

Mass of wheat filling the container obtains equation (77):

$$m_1 = 2bh\rho = 2.448 * 10^4 \text{ kg}. \quad (77)$$

To calculate the dynamic stresses in the load-handling frame construction of the stationary hoist under development, the frame calculation scheme is used. Load impact force obtains equation (78):

$$P=m*9.81*10^{-3}=0.793 \text{ kN}. \quad (78)$$

In calculating the dynamic coefficient for impact load, it can be assumed that the kinetic energy of the striking body is completely converted into the potential energy of deformation of the elastic system. This results in equation (79):

$$T = U_D. \quad (79)$$

Since by the moment of deformation termination, the striking body will have travelled the path $H + \delta_D$, its energy reserve will be determined by the work A_D, which it performs, and is equal to equation (80):

$$T = A_D = Q(H + \delta_D). \quad (80)$$

Now, we determine U_D. In static deformation, the potential energy U_C is equal to half the product of the force acting on the system by the corresponding deformation (see equation (81)):

$$U_C = \frac{1}{2} Q\delta_C. \quad (81)$$

Hooke's law is used to calculate the static strain δ_C in the impacted section. This law can be written in general terms as $c = Q/\delta_C$ or $Q = c \cdot \delta_C$, where c is the is the coefficient of proportionality, also called the stiffness of the system, used to measure the relationship between force and strain. The coefficient depends on factors such as material properties, shape and size of the body, type of deformation and position of the impacted cross-section.

DOI: http://dx.doi.org/10. 17509/xxxx.xxxx
p- ISSN 2776-6098 e- ISSN 2776-5938

For simple tension or compression, the strain is $\delta_C = \Delta l_C$, and $c = \frac{49EJ}{i^3}$; for bending of a beam hinged at the ends by a concentrated force Q in the middle of the span, $\delta_C = f_{Cmax} = \frac{Qi^3}{48EJ}$ and $c = \frac{48EJ}{i^3}$; and so forth. Thus, the equation for calculating the energy is reformulated in equation (82):

$$\mathrm{U_C} = \frac{1}{2}\mathrm{Q}\delta_\mathrm{C} = \frac{\mathrm{c}}{2}\delta_\mathrm{c}^2. \tag{82}$$

The equation for calculating energy is based on two conditions:

(i) Hooke's law describes the relationship between force and strain;

(ii) force Q, stress p_C , and strain δ_C increase gradually from zero to their final value.

During impact, the strain increases gradually over an extremely short period of time until it reaches its final value. Along with the increase in strain, the stresses p_D also increase in parallel. The P_D reaction caused by the fallen load Q and acting on system C arises due to the deformation δ_D that occurs in the material of the system. The P_D reaction gradually increases with increasing strain δ_D and reaches its maximum value. Provided that the stresses induced by this reaction do not exceed the material proportionality limit, it obeys Hooke's law (see equation (83)):

$$\delta_\mathrm{D} = \mathrm{P_D}/\mathrm{c}, \tag{83}$$

where c is the is the coefficient of proportionality. It retains its value even after the impact.

Thus, equation (81) for calculating the deformation energy of system C during impact is valid since its basic prerequisites is the validity of Hooke's law and the gradual growth of force and deformation is the are also preserved under dynamic loads (**Figures 11** and **12**).

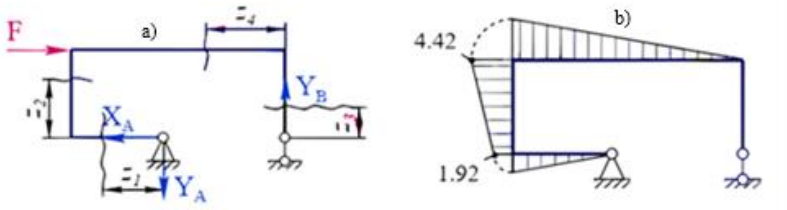

Figure 11. Calculation scheme for determining deformation along the X axis (a) and resulting deformation diagram (b)

Figure 10a illustrates the deformation profile of the frame along the *X*-axis, especially in response to horizontal forces. This part visually represents how different regions of the frame experience displacement, highlighting areas where deformation is most pronounced. **Figure 10b** shows the magnitude or direction of deformation along the *X*-axis in a quantitative or graphical format, further detailing the response of the frame to horizontal loading. This information helps to identify specific areas where reinforcement may be required.

Figure 12a shows the computational scheme of the model used to estimate the vertical deformation along the Y-axis. An overview of the structural configuration of the frame and loading conditions is presented, providing a framework for analyzing vertical displacements. **Figure 12b** presents computational results illustrating the extent and distribution of vertical strain across the frame under large vertical loads. This visual representation identifies areas where vertical displacements are most significant.

DOI: http://dx.doi.org/10. 17509/xxxx.xxxx
p- ISSN 2776-6098 e- ISSN 2776-5938

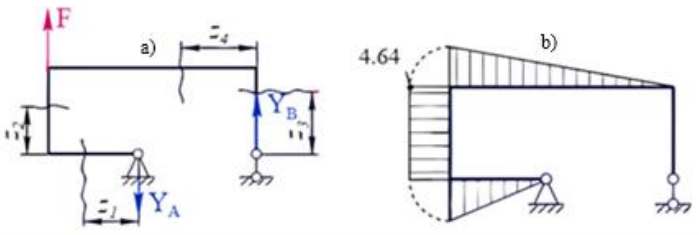

Figure 12. Calculation scheme for determining deformation along the Y axis (a) and resulting deformation diagram (b)

Thus, the equation for the potential energy U_D during the impact will be in the same form as in the case of a static loading of the system *C* taking into account the force of inertia P_D, as shown in equation (84):

$$U_D = \frac{1}{2} P_D \delta_D = \frac{c}{2} \delta_D^2 = \frac{Q}{2\delta_C} \delta_D^2. \quad (84)$$

Here it is taken into account that $c = Q/\delta_C$ and applying the values of *T* and U_D to equation (79), we obtained equation (85):

$$Q(H + \delta_D) = \frac{Q}{2\delta_C} \delta_D^2, \quad (85)$$

or equation (86) is:

$$\delta_D^2 - 2\delta_C \delta_D - 2H\delta_C = 0. \quad (86)$$

Therefore equation (87) is:

$$\delta_D = \delta_C \pm \sqrt{\delta_C + 2H\delta_C}. \quad (87)$$

The dynamic coefficient is determined by the equation (88):

$$K_D = 1 + \sqrt{1 + \frac{2H}{\delta_C}}. \quad (88)$$

Equation (88) applies only when the mass of the elastic body under impact is small and can be ignored. If the mass of the body is needed to be taken into account in equations (89), (90):

$$K_D = 1 + \sqrt{1 + \frac{2P}{\delta_C(1 + \frac{m_{rm}}{m_1})}}, \quad (89)$$

where m_1 is the mass of the falling load; m_{rm} is the reduced mass of the body on which the impact occurs. In this case, equation (90) is

$$m_{rm} = \alpha m, \quad (90)$$

where *m* is the true mass of the body that is distributed over its volume; α is the coefficient that allows distributed mass to be reduced to an equivalent point mass.

The coefficient α is determined by comparing the kinetic energy of the body with the total mass, taking into account distributed and point masses. This allows the mass of the body under impact to be taken into account. The dynamic calculation of the frame is performed by changing the angle of the tilt α and substituting the value of the dynamic force *P* instead of the static load (see equations (91) and (92)):

$$\alpha = -90° = -1.571 \text{ rad}, \quad (91)$$

DOI: http://dx.doi.org/10. 17509/xxxx.xxxx
p- ISSN 2776-6098 e- ISSN 2776-5938

$$F = \frac{P}{8} = 0.099 \text{ kN}. \quad (92)$$

The deformation of the frame from the static load in the direction of the force *F* in the *X* and *Y* axis is determined. Then the displacement values are determined using Mora's integral and the total deformation is calculated (93):

$$\Delta_{F_x} = 1.815,$$

$$\Delta_{F_y} = 4.363,$$

$$\Delta_F = \sqrt{\Delta_{Fx}^2 + \Delta_{Fy}^2} = 4.725. \quad (93)$$

Reduced mass of the frame at the point of impact is in equations (94)-(96):

$$m_1 = \frac{17}{35} * 7700 * 225 * 10^{-4} * 2(h + b) = 1.437 * 10^3 \text{ kg}, \quad (94)$$

$$\Delta_{st} = \frac{\Delta_F}{EI_{xD}} = 7.305 * 10^{-5} m, \quad (95)$$

$$Kd = 1 + \sqrt{1 + \frac{2h_0}{\Delta_{st}(1 + \frac{m_1}{m})}}, \quad (96)$$

where K_d = 102.326 is the dynamic coefficient that increases the dynamic stress. Dynamic stress obtains equation (97):

$$\sigma_d = Kd\sigma_{ст} = 39.749 \text{ MPa}. \quad (97)$$

The results of calculations of container filling time and dynamic stresses arising during loading in the construction of the load-handling frame of a stationary hoist are presented. The calculations were performed using the MathCad software environment and are presented in **Table 4**.

Table 4. Calculation results performed in the MathCad application program.

Trials	1	2	3	4
Hole radius of the hopper opening, *R*, cm	10	15	20	25
Container filling time, t_V, min	20.397	6.044	2.55	1.305
Dynamic stress, σ_d, MPa	12.002	39.749	90.989	168.608

After theoretical research, the obtained results of calculations (see **Tables 3 and 4**) performed in the MathCad application software environment are plotted on a grid of rectangular coordinates and connected by their points in dependence. **Figures 13-15** show the dependences of static stresses on the acting loads according to 32 calculations (see **Table 3**) for the tested positions 2, 3, and 4. The curves make it clear that static stresses (σ_i, MPa), which occur in the construction of the load-handling frame of the stationary hoist, increase as the loading (F_i/S, MPa) on it increases.

Figure 13 illustrates a discernible trend whereby an increase in tilt angle is accompanied by a corresponding rise in static stress, particularly at elevated loads. This indicates that operating the frame at greater angles exerts greater strain on the structure, which may result in accelerated deterioration. To address this issue, the frame design could incorporate supports or mechanisms that facilitate the more uniform distribution of the load, particularly at extreme tilt angles.

DOI: http://dx.doi.org/10. 17509/xxxx.xxxx
p- ISSN 2776-6098 e- ISSN 2776-5938

From **Figure 14**, the static stresses at a 30° tilt are significantly lower than those at steeper angles. This indicates that moderate tilts result in a more balanced load distribution, reducing the overall strain on the frame. For operations where stability and longevity are critical, maintaining a tilt angle close to 30° could be an optimal solution, as it places less stress on the structure while still allowing for efficient loading.

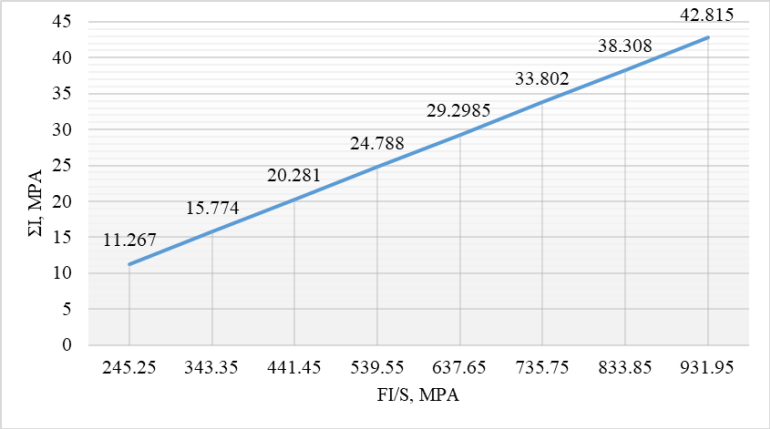

Figure 13. Dependence of static stresses (σ_i, MPa) on acting loads (F_i/S, MPa) at test position 2 (at 60°).

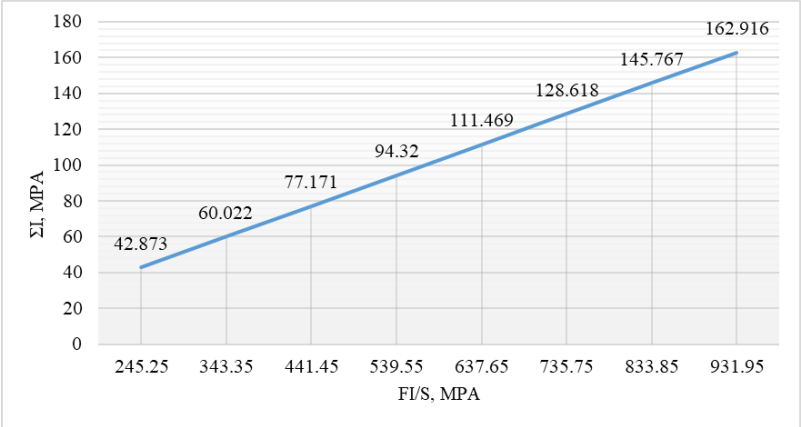

Figure 14. Dependence of static stresses (σ_i, MPa) on acting loads (F_i/S, MPa) at test position 3 (at 30°).

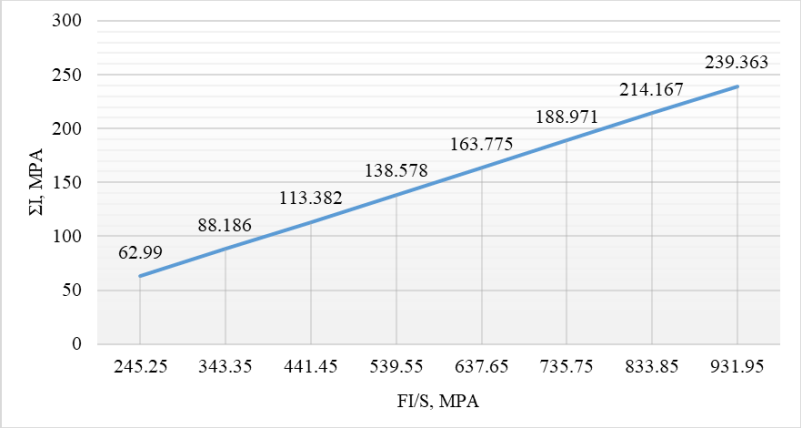

Figure 15. Dependence of static stresses (σi, MPa) on acting loads (Fi/S, MPa) at test position 4 (at 0 °).

DOI: http://dx.doi.org/10. 17509/xxxx.xxxx
p- ISSN 2776-6098 e- ISSN 2776-5938

The lowest static stresses are observed when the container is in a horizontal position, confirming that a level configuration minimizes strain on the frame. Therefore, horizontal loading should be the preferred orientation for operations where minimizing stress and maximizing frame longevity are key concerns. By designing the system to favor horizontal positioning, the structure operates under the least strain, reducing maintenance costs and extending the life of the equipment.

Figure 16 shows the dependence of dynamic stresses on the hole radius of the downcomer pipes of the loading hopper according to 4 calculations (Table 4) for test position 1 (when the tilt angle of the container is 90°), with the implementation of 4 changes of the radius of the downcomer pipes.

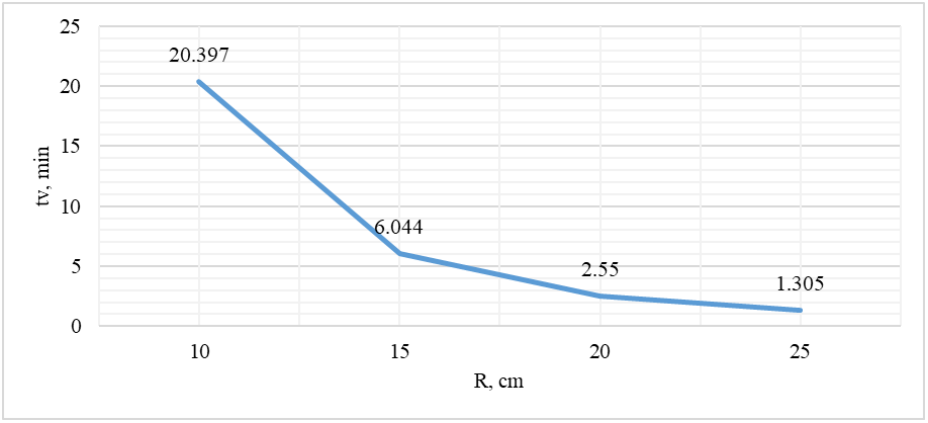

Figure 16. Relationship between the hole radius of the downcomer pipes of the loading hopper and the time required to fill the hopper.

According to the curve in **Figure 16**, with the increase of hole radius of the downcomer pipes of the loading hopper, the container filling time and dynamic stresses also increase. **Figure 17** shows the dependence of the container filling time on the hole radius of the downcomer pipes of the loading hopper according to 4 calculations (see **Table 4**) for test position 1 (when the tilt angle of the container is 90°), with the implementation of four changes of the radius of the downcomer pipes.

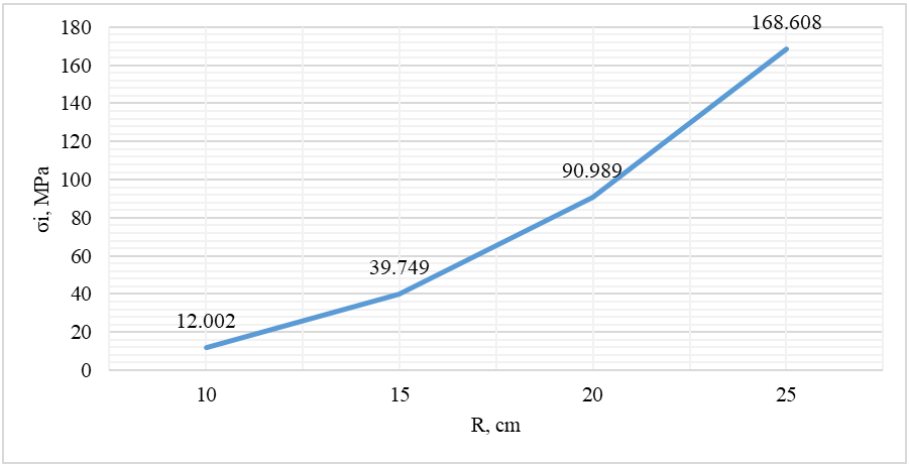

Figure 17. Dependence of dynamic stresses on the hole radius of the downcomer pipes of the loading hopper.

The data presented in **Figure 17** demonstrate that an increase in the radius of the downcomer pipe is accompanied by a corresponding rise in dynamic stresses. This suggests

DOI: http://dx.doi.org/10. 17509/xxxx.xxxx
p- ISSN 2776-6098 e- ISSN 2776-5938

that larger pipe diameters, while facilitating faster filling times, exert greater stress on the frame, which could potentially result in structural fatigue over time. It is essential to strike a careful balance between hopper size and stress management in order to optimize the filling process without compromising the integrity of the frame. Modifications to the configuration of the downcomer pipes or reinforcement of the frame in pivotal locations may prove an effective means of alleviating the heightened stress levels associated with larger pipe diameters.

The findings of this study illustrate that the load-handling frame of the stationary hoist, designed for loading grain into containers, demonstrates structural integrity under both static and dynamic stresses. The maximum static stress observed in the frame did not exceed the permissible limit of 250 MPa, thereby confirming the frame's strength and durability. The results of the dynamic stress analysis indicated that the stresses increased in conjunction with an expansion in the diameter of the downcomer pipes, which also resulted in a reduction in the time required to fill containers. However, this increase in efficiency was accompanied by an increase in stress on the structure. These findings indicate that a careful optimization process is required in order to achieve an equilibrium between operational efficiency and the structural longevity of the hoist. The mathematical modeling and experimental data substantiate the conclusion that the hoist design is capable of accommodating significant loads while maintaining stability, thereby rendering it suitable for efficient grain loading operations.

4.2. Discussion

Research and development of technologies related to grain, its loading, transport, and storage are important to the agricultural and food industries. These technologies play a crucial role in ensuring the efficient and safe transport of grain from producer to consumer, as well as preserving its quality and minimizing losses in the process. One of the key objectives of research in this area is to improve the productivity and efficiency of grain transport. As the world population grows and the demand for food increases, there is a need for faster and more efficient delivery of grain from the point of production to consumers (Galkin *et al.,* 2019). Technological innovations such as automated loading and unloading systems, optimized logistics, and the usage of modern vehicles can significantly reduce the time and costs of grain transport (Jakubik *et al.,* 2017; Nussibaliyeva *et al.,* 2024). Some studies are a significant contribution to the understanding of grain transportation and its role in the marketing system of the grain sector. They draw attention to the importance of transport in determining the prices of grain crops, where the prices received by farmers often depend on the cost of transporting grain to the central market. Some researchers (Jiang *et al*., 2022) gave recommendations to improve management and forecasting in the grain haulage industry in Canada, which is important for the sustainability and development of this industry and may be useful in other countries.

In addition, the development of grain-related technologies helps to solve problems related to the preservation of grain quality. During transportation and storage, grain is exposed to various factors such as humidity, temperature, mechanical stress, and pests (Sinoimeri *et al.,* 2024; Bulgakov *et al.,* 2020). The use of modern methods and technologies such as controlled atmospheres, specialized packaging materials and monitoring sensors can manage these factors and ensure that grain quality is maintained throughout the entire transport and storage cycle. Some researchers present a prototype of a mobile container that can be used to transport and store crops, vegetables, and even fruits under optimal conditions. This new electronic device offers a solution that can help to preserve the quality and freshness of

DOI: http://dx.doi.org/10. 17509/xxxx.xxxx
p- ISSN 2776-6098 e- ISSN 2776-5938

agricultural products during transport and storage. Some researchers (Dyer *et al*., 2023) presented a study aimed at evaluating the feasibility of modernizing anchorage points for safe entry into a grain store using the finite element method. Some researchers (Horabik *et al*., 2016) were also engaged in developments in this field. Their study performs experiments and modeling by the discrete element method to study the distribution of static load on the bottom of a shallow model silo. The effect of the filling method, seed size, and seed ratio on the radial distribution of vertical pressure at the bottom of a shallow silo was studied. The computationally efficient model (Liu *et al*., 2022) allows for more efficient and accurate prediction of grain profile changes inside the container, as well as predict the possible dispersion of grain materials. The results of this research demonstrate the applicability of the model in a real-time environment and validate its accuracy using experimental data.

At another point, some researchers (Zhao *et al*., 2020) investigated the problem of organizing the assembly of railway containers using intermodal rail-sea transport. The main aim of the study is to maximize the efficient use of resources and provide an environmentally sustainable perspective to reduce the cost of the assembly process. In the assembly process, a model of the organization of the railway transport of containers was created, taking into account the location of different central stations and goods. A genetic algorithm was used to solve the model, taking into account specific practical situations such as capacity. Through calculations and simulations, it was found that the model and algorithm are functional and efficient. According to the results, the requirements of optimal resource use and environmental protection can be successfully fulfilled, which play an important role in China's sustainable development. Although this study is based on China's national conditions, the principle of universality has been taken into account in the development of the model. Therefore, it is sufficient to replace the relevant data to disseminate and apply the model. However, it should be noted that this study is limited to unidirectional transport, and the resources of vehicles in the port were not considered. Future research should focus on bidirectional transport and investigate the use of empty vehicles in more detail. Future studies may also include the practical implementation of large-scale central stations and ports (Otenko *et al.,* 2023).

The article (Bruns & Knust, 2012) describes three formulations of the integer linear programming problem for solving the train load scheduling problem in multimodal container terminals. The main aim is to maximize train usage and minimize set-up and transportation costs in the terminal. Unlike previous approaches, the formulations also include constraints on the weight of wagons. They demonstrate that this problem can be solved quickly (even with non-commercial IP solvers) for real data. The results of the first two formulations show that it is possible to use the bootstrapping patterns established by companies to formulate weight constraints. However, modeling the weight constraints directly using suitable equations proved to be more efficient. The third formulation was solved in a few seconds. In addition, this formulation is more flexible and does not require pre-calculation of a set of acceptable load samples. Finally, they plan to test the developed formulations in practice, taking into account the peculiarities of each particular terminal (e.g., the presence of dangerous goods, height restrictions of cargo units, or different assignments of wagons within the same train). The paper (Ambrosino *et al.*, 2013) studied and compared different train loading policies using different storage strategies in a container terminal. They test nine different policies based on a combination of sequential, non-sequential, and partially sequential train loading and different container storage strategies. The results of the analysis show that the preferred loading and storage strategies depend on the specific terminal and its objectives, and a future study will analyze the different scenarios in more depth.

DOI: http://dx.doi.org/10. 17509/xxxx.xxxx
p- ISSN 2776-6098 e- ISSN 2776-5938

Some researchers (Ng & Talley, 2020) address the issue of optimizing the use of rail trains for container transport in marine terminals, especially using double formations. The use of rail transport is important to improve the sustainability and efficiency of container transport to and from marine terminals, especially with the increasing size of ships (Musayev *et al.,* 2022; Kashkanov & Moskaliuk, 2024). A binary linear optimization model has been developed to optimize the space utilization on railway trains. To verify the effectiveness of the model, realistic tests were conducted, which led to interesting observations. For example, it was found that if the number of railway hubs is limited to one railway track, the space usage on railway trains decreases significantly. On the other hand, if multiple railway hubs per track are allowed, the space usage on the trains can be significantly increased (Kuzmenko *et al.,* 2021). It has also been found that as the number of containers increases, e.g., due to the use of large capacity ships, the usage of one railway hub per track becomes less and less optimal. Optimal loading plans can be obtained if the number of containers is large enough. This means that the use of large-capacity ships can facilitate the use of railway trains, even if this leads to sub-optimal methods. The proposed model allows the most important parameters to be taken into account when developing optimal loading plans for railway trains. However, for more accurate optimization, an extension of the model to account for less common container types such as tanks and dangerous goods can be considered. Optimization of container loading and ship departure planning can also be considered to ensure that the right containers are available at the right time.

The solutions developed by the above-mentioned reports can also be used in Kazakhstan to increase transport flows in the region. They propose models to optimize logistics processes and increase resource efficiency in the transport system. This will allow Kazakhstan to become another logistics hub and strengthen its economic position in the region. However, it should be noted that the implementation of such projects should take into account environmental and social aspects to ensure sustainable development of the region.

The findings show the necessity of incorporating both static and dynamic stresses into the design of load-handling systems for grain transportation. The findings indicate that an increase in the diameter of downcomer pipes results in a reduction in container filling time; however, this also introduces higher dynamic stresses, necessitating careful design considerations to achieve an optimal balance between efficiency and structural integrity. The results offer a practical insight into the potential for improving grain loading operations, with the possibility of extending the applications beyond Kazakhstan to other major grain-exporting regions. This approach not only enhances operational efficiency but also ensures that safety standards are met, thereby making a valuable contribution to the global grain logistics industry.

5. CONCLUSION

As a result of the research, the initial data for mathematical modeling were determined:

(i) the MathCad application program was selected for analytical calculation;
(ii) four test positions of the load-handling frame of the developed stationary hoist were selected according to the technology of loading works;
(iii) the number of static stress calculations was determined for the selected positions;
(iv) the calculation scheme for determining static stresses was proposed;
(v) the number of calculations to determine the minimum time of filling the container and dynamic load at the test position 1 (at the angle of the tilt of the container is 90°), with the implementation of 4 changes in the radius of the downcomer pipes of the loading hopper.

DOI: http://dx.doi.org/10. 17509/xxxx.xxxx
p- ISSN 2776-6098 e- ISSN 2776-5938

Additionally, the static stresses in the construction of the load-handling frame of the stationary hoist under development have been calculated. For the first time, transient stiffness coefficients of the system were introduced, taking into account changes in the geometric characteristics of the cross-sections of the load-handling frame sections, and these coefficients are equal to μ = 0.014; v = 0.029; and = 0.072. When calculating Mora's integral, the method of direct integration is used to calculate the frame displacements accurately. The calculation of a statically indeterminable load-handling frame by the force method in matrix form was carried out, which allowed calculation of the effectively for (made it possible to effectively calculate) the systems having a large degree of static indeterminacy and a significant number of loading sections.

Thus, the obtained values of maximum normal stresses in the construction of the load-handling frame fully satisfy the condition of strength, ensuring that the maximum stresses will not exceed the permissible stress. In addition, modeling of the container filling process was performed by calculating the time and speed of its filling depending on the mass of the falling bulk medium. The dynamic stresses occurring in the load-handling frame construction of the stationary hoist under development were calculated. The dynamic coefficient λ dependent on the height of the fall was calculated and the dynamic stresses during the filling of the container were determined based on the impact theory. Furthermore, during processing and analysis of the results of mathematical modeling performed in the MathCad software environment, the dependences of static stresses (σi, MPa) on the acting loads (Fi/S, MPa) for four tested positions were obtained, the relationship between the time of container filling and the hole radius of the downcomer pipes of the loading hopper was found, and the data on the relationship of dynamic stresses with hole radius of the downcomer pipes of the loading hopper were obtained.

This study presents a comprehensive evaluation of both static and dynamic stresses in the design of a stationary hoist system for grain loading. The integrated mathematical model developed here represents a significant advancement in the field of grain transportation systems, providing more accurate predictions and practical solutions for optimizing such systems. The broader implications of this research are threefold: firstly, it has the potential to improve global agricultural logistics; secondly, it has the potential to reduce costs; and thirdly, it has the potential to enhance the competitiveness of grain exports from Kazakhstan and other key regions. Further research should investigate the environmental and cost-saving benefits of such optimizations in greater depth, particularly in the context of sustainable agricultural practices.

6. ACKNOWLEDGMENT

This research has been funded by the Science Committee of the Ministry of Science and Higher Education of the Republic of Kazakhstan (Grant No. AP14869550)..

7. AUTHORS' NOTE

The authors declare that there is no conflict of interest regarding the publication of this article. Authors confirmed that the paper was free of plagiarism.

8. REFERENCES

Ambrosino, D., Caballini, C., and Siri, S. (2013). A mathematical model to evaluate different train loading and stacking policies in a container terminal. *Maritime Economics and Logistics*, *15*, 292-308.

Barbieri, E., and Botto, L. (2022). Peeling under large bending deformations: Follower versus fixed loads. A unified approach for concentrated or distributed loads. *International Journal of Solids and Structures*, *241*, 111450.

Bruns, F., and Knust, S. (2012). Optimized load planning of trains in intermodal transportation. *OR Spectrum*, *34*(3), 511-533.

Bulgakov, V., Nikolaenko, S., Holovach, I., Adamchuk, V., Kiurchev, S., Ivanovs, S., and Olt, J. (2020). Theory of grain mixture particle motion during aspiration separation. *Agronomy Research*, *18*(1), 18-37.

Dyer, M., Gorucu, S., Bock, R., Thomas, R., Liu, J., and Fetzer, L. (2023). Case study: Modeling a grain bin for safe entry retrofit. *Safety*, *9*(2), 28.

Galkin, A., Obolentseva, L., Balandina, I., Kush, E., Karpenko, V., and Bajdor, P. (2019). Last-mile delivery for consumer driven logistics. *Transportation Research Procedia*, *39*, 74-83.

Horabik, J., Parafiniuk, P., and Molenda, M. (2016). Experiments and discrete element method simulations of distribution of static load of grain bedding at bottom of shallow model silo. *Biosystems Engineering*, *149*, 60-71.

Ibatov, M.K., Balabaev, and O.T., Kassymzhanova, A.D. (2021). Studying the method of loading containers by testing in the software environment. *Material and Mechanical Engineering Technology*, *4*, 35-38.

Ilesaliev, D.I., Azimov, F.K., Shikhnazarov, J.A., and Dehkonov, M.M. (2021). Intermodal and multimodal technologies for transportation of grain cargo. *Silk Road Transport*, *4*, 54-69.

Jakubik, P., Kerimkhulle, S., and Teleuova, S. (2017). How to anticipate recession via transport indices. *Ekonomicky Casopis*, *65*(10), 972-990.

Jiang, S., Nolan, J., and Wilson, W.W. (2022). Exit decisions in the Canadian grain elevator industry. *Journal of Industry, Competition and Trade*, *22*, 1-19.

Kashkanov, A., and Moskaliuk, M. (2024). Methods of justification of spare parts stocks in the transport process management system. *Journal of Mechanical Engineering and Transport, 10*(1), 68-74.

Kassymzhanova, A.D., Ibatov, M.K., Balabayev, O.T., Donenbaev, B.S., and Ilessaliyev, D.I. (2022). Experimental study of maximum stresses in the stationary hoist design in the ANSYS software environment. *Communications*, *24*(4), 310-318.

Kuzmenko, O.V., Dotsenko, T.V., and Skrynka, L.O. (2021). Economic and mathematical modeling of the effectiveness of the national system for countering cyber fraud and criminal proceeds legalisation based on survival analysis methods. *Scientific Bulletin of Mukachevo State University. Series "Economics"*, 8(1), 144-153.

Liu, Z., Jiang, C., Evans, J.T., Dhamankar, S., Heusinger, L.J., Shaver, G.M., and Puryk, C.M. (2022). A computationally efficient model for granular material piling in a container. *Computers and Electronics in Agriculture*, *194*, 106692.

Lupoiu, F., Pleşca, A.T., Gabor, G., and Chiriac, G. (2020). A new solution of electronic device proposed for cereals, vegetables and fruits storage. In 2020 *International Conference and Exposition on Electrical and Power Engineering (EPE)* (pp. 403-406). Iasi: IEEE.

DOI: http://dx.doi.org/10. 17509/xxxx.xxxx
p- ISSN 2776-6098 e- ISSN 2776-5938

Mizanbekov, I., Bekbosynov, S., and Lytkina, L. (2023). Factors affecting the cost of grain transportation in the conditions of Northern Kazakhstan. *Bulletin of the L.N. Gumilyov Eurasian National University*, *142*(1), 137-145.

Musayev, J., Zhauyt, A., Bahtiyar, B., Kibitova, R., Kazhet, K., Kussyov, A., and Kabylkarim, A. (2022). Analysis of dynamic instability of the wheel set of a railway vehicle using the method of generalized hill determinants. *Vibroengineering Procedia*, *41*, 186-190.

Ng, M., and Talley, W.K. (2020). Rail intermodal management at marine container terminals: Loading double stack trains. *Transportation Research Part C-Emerging Technologies*, *112*(3), 252-259.

Nussibaliyeva, A., Sergazin, G., Tursunbayeva, G., Uzbekbayev, A., Zhetenbayev, N., Nurgizat, Y., Bakhtiyar, B., Orazaliyeva, S., and Yussupova, S. (2024). Development of an artificial vision for a parallel manipulator using machine-to-machine technologies. *Sensors*, *24*(12), 3792.

Otenko, V., Malyarets, L., Barannik, I., and Budarin, O. (2023). Determining the economic sustainability reserve of economic entities in modern operating conditions. *Economics of Development*, *22*(2), 8-18.

Ruzmetov, Y., and Valieva, D. (2021). Specialized railway carriage for grain. *E3S Web of Conferences*, *264*, 05059.

Sinoimeri, D., Teta, J., Prifti, V., and Lazaj, A. (2024). Information technology in supply chain management. case study. *Lecture Notes on Multidisciplinary Industrial Engineering*, *2090*, 35-44.

Wilson, W.W., and Dahl, B. (2011). Grain pricing and transportation: Dynamics and changes in markets. *Agribusiness*, *27*(4), 420-434.

Zhao, J.H., Zhu, X.N., and Wang, L. (2020). Study on scheme of outbound railway container organization in rail-water intermodal transportation. *Sustainability*, *12*(4), 1519.

DOI: http://dx.doi.org/10. 17509/xxxx.xxxx
p- ISSN 2776-6098 e- ISSN 2776-5938